VERIFICATION OF GOAL-ORIENTED HP-ADAPTIVITY

M. Paszyński [1], L. Demkowicz, D. Pardo,

Institute for Computational Engineering and Sciences
The University of Texas at Austin

Abstract

The paper presents calculations for the radiation of a loop antenna wrapped around a metallic cylinder into a conductive medium. The problem has been solved analytically by using Fourier transform and Bessel functions. The evaluation of the analytical solution, involves the use of exponentially scaled Bessel functions, and FFT to evaluate inverse Fourier transform, with all computations done in MATLAB. The analytical solution has been used to validate a goal-oriented *hp* adaptive strategy based on a simultaneous solution of a dual problem, and an *hp* strategy based on minimizing the projection-based interpolation error of a reference solution.

Key words: Automatic *hp*-adaptivity, goal-oriented adaptivity, numerical evaluation of Fourier transform, radiation of a loop antenna

Acknowledgment

The work of the second author has been supported by Air Force under Contract F49620-98-1-0255. Helpful discussions with Dr George Cardwell are gratefully acknowledged.

1 Introduction

The automatic goal driven *hp* adaptivity has been used to solve challenging problems in computational electromagnetics [2]. In this paper we formulate and solve, both analytically and numerically, a problem of radiation of a loop antenna wrapped around a metallic mandrell into a conductive medium. The problem has been solved numerically by using goal-oriented *hp* adaptive code [2] with a solution evaluated at a sequence of points. The main goal of this paper is to solve the same problem analytically in terms of Bessel functions and inverse Fourier transform, to verify the goal-oriented *hp* adaptive computations. Main challenges include:

- The dynamic range of the solution (ratio between the maximum and minimum values of the solution within the domain of interest) spans 14 digits.

[1]On leave from *AGH University of Science and Technology, Department of Computer Methods in Metallurgy, Cracow, Poland*, e-mail: maciek@ices.utexas.edu, mpaszynski@hotmail.com

- In order to evaluate the analytical solution, one must overcome difficulties with the numerical evaluation of the (inverse) Fourier Transform by using FFT. This requires the use of a smooth truncating function to enable exponential convergence of the FFT based quadrature.

The presented considerations are relevant to modeling of logging devices [3]. The high accuracy of solutions for this class of problems is required in the area of logging while drilling inverse problems. The presentation is done in a tutorial style, explaining all mathematical details, with beginning graduate students in mind.

2 Statement of the problem

The following radiation problem is relevant to drilling technologies [3]. A loop antenna, wrapped around an infinite metallic cylinder, radiates into a conductive homogeneous medium, as illustrated in Fig. 1. The radius of the metallic mandrell is a, and there is a non-zero distance $b-a$ between the metallic mandrell and the loop antenna.

We start with the time-harmonic Maxwell equations,

$$\nabla \times \left(\frac{1}{\mu} \nabla \times E\left(x,y,z,t\right) \right) + \epsilon \frac{\partial^2 E\left(x,y,z,t\right)}{\partial t^2} + \sigma \frac{\partial E\left(x,y,z,t\right)}{\partial t} = -\frac{\partial J^{imp}\left(x,y,z,t\right)}{\partial t}, \tag{2.1}$$

where μ stands for a permeability, σ is conductivity, ϵ denotes permittivity, and J^{imp} is an imposed current.

Fourier transform with respect to time t leads to,

$$\nabla \times \left(\frac{1}{\mu} \nabla \times E\left(x,y,z,\omega\right) \right) - \left(\omega^2 \epsilon - i\omega\sigma \right) E\left(x,y,z,\omega\right) = -i\omega J^{imp}\left(x,y,z,\omega\right). \tag{2.2}$$

We switch now to the axisymmetric formulation in the cylindrical system of coordinates with z axis located on the axis of the metallic mandrell, and the origin at the center of the loop antenna. The only non-zero component of the electric field is the angular component E_ϕ. Components $E_r = E_z = 0$, due to the axisymmetry of the problem. Maxwell equations (2.2) reduce to a single elliptic problem,

$$\frac{1}{\mu} \left(-\frac{\partial^2 E_\phi}{\partial z^2} + \frac{1}{r^2} E_\phi - \frac{1}{r} \frac{\partial E_\phi}{\partial r} - \frac{\partial^2 E_\phi}{\partial r^2} \right) - \left(\omega^2 \epsilon - \sigma i\omega \right) E_\phi = -i\omega J^{imp}. \tag{2.3}$$

We assume that the imposed current is given by a Dirac delta $J^{imp}\left(x,\phi,z\right) = \delta\left(r-b\right)\delta\left(z-0\right)e_\phi$, where e_ϕ is the angular unit vector in the cylindrical system of coordinates.

For the numerical computations we have set $a = 0.0254$ [m], $b = 0.03048$ [m], $\omega = 2\pi f$ where the frequency $f = 2 \cdot 10^6$ [Hz], $\mu = \mu_0 = 4\pi 10^{-7}$ is the free space permeability and $\epsilon = \epsilon_0 = \frac{1}{36\pi} 10^{-9}$ is the free space permittivity. The metallic mandrell is assumed to be a perfect conductor. The conductivity of the medium is $\sigma = 1$ [S/m].

The formulation can be transformed into a non-dimensional form, by defining,

$$\mu_r = \frac{\mu}{\mu_0} \qquad \epsilon_r = \frac{\epsilon}{\epsilon_0} \qquad x_r = \frac{x}{d} \qquad E_r = \frac{E}{E_0}, \tag{2.4}$$

where μ_r is the dimensionless permeability, ϵ_r is the dimensionless permittivity, $d = b - a$ is the spatial scale and $E_0 = 1$ is the solution scale. These are the four basic scaling factors. The remaining quantities are transformed into a dimensionless form by defining,

$$\Omega = \omega\sqrt{\epsilon_0\mu_0}d \qquad \Sigma = \sigma\sqrt{\frac{\mu_0}{\epsilon_0}}d \qquad J_r^{imp} = \frac{J^{imp}\sqrt{\frac{\mu_0}{\epsilon_0}}d}{E_0}, \tag{2.5}$$

where Ω is a non-dimensional wave number, Σ is a non-dimensional conductivity, and J_r^{imp} is a non-dimensional imposed current.

A potential pitfall is to try to solve the equation (2.3) by using a separation of variables technique. There are two issues:

- The separation of variables technique can be applied in a rigorous way only to a problem resulting in a Sturm-Liouville system [4]. This requires the domain to be bounded in at least one direction. Our domain of consideration is unbounded in both r and z.
- Equation (2.3) is a distributional equation, with a regular distribution part associated with the left-hand side, and a non-regular Dirac delta distribution on the right-hand side.

We begin by applying the Fourier transform with respect to z variable.

The Fourier transform of a non-regular distribution is defined by generalizing the classical Fourier transform. We start from the Plancherel theorem [11] which states that the L^2 scalar product of two functions is equal to the L^2 scalar product of its Fourier transforms. This can be interpreted in terms of distributions as,

$$< FT\left(R_f\right), \hat{\phi} >=< R_f, FT^{-1}\left(\hat{\phi}\right) >, \tag{2.6}$$

where $FT\left(R_f\right)$ is the Fourier transform of a regular distribution R_f associated with function f, $\hat{\phi}$ is the Fourier transform of testing function ϕ, and $FT^{-1}\left(\hat{\phi}\right)$ is the inverse Fourier transform of $\hat{\phi}$. Applying (2.6) to the Dirac delta, we get,

$$< FT\left(\delta\right), \hat{\phi} >=< \delta, FT^{-1}\left(\hat{\phi}\right) >= FT^{-1}\left(\hat{\phi}\left(0\right)\right) = \frac{1}{\sqrt{2\pi}}\int_{-\infty}^{+\infty}\hat{\phi}\left(\omega\right)d\omega =< R_{\frac{1}{\sqrt{2\pi}}}, \hat{\phi} >, \tag{2.7}$$

with $R_{\frac{1}{\sqrt{2\pi}}}$ denoting the regular distribution associated with factor $\frac{1}{\sqrt{2\pi}}$.

Fourier transforming with respect to z variable, we obtain,

$$\hat{E}_\phi\left(r,\hat{z}\right)\left(-\alpha^2 + \frac{1}{r^2}\right) - \frac{1}{r}\frac{\partial\hat{E}_\phi\left(r,\hat{z}\right)}{\partial r} - \frac{\partial^2\hat{E}_\phi\left(r,\hat{z}\right)}{\partial r^2} = -\mu i\omega\frac{1}{\sqrt{2\pi}}\delta\left(r-b\right), \tag{2.8}$$

where we have denoted $-\alpha^2 = \hat{z}^2 - \mu\left(\omega^2\epsilon - \sigma i\omega\right)$. All terms in (2.8) must be understood as regular distributions, except for the Dirac delta term, and all derivatives must be understood in the distributional sense.

With the Dirac delta concentrated at point b in the domain, the distributional derivative of a regular distribution $\frac{\partial R_{\hat{E}}}{\partial r}$ is a sum of a regular distribution associated with the classic derivative $\hat{E}'_\phi = R_{\hat{E}'_\phi}$, and a jump term $[\hat{E}_\phi(b)]$ times a Dirac delta at point b [6],

$$\frac{\partial R_{\hat{E}}}{\partial r} = R_{\hat{E}'_\phi} + [\hat{E}_\phi(b)]\delta(r-b). \tag{2.9}$$

Consequently, the second distributional derivate equals,

$$\frac{\partial}{\partial r}\left(\frac{\partial R_{\hat{E}}}{\partial r}\right) = \frac{\partial}{\partial r}\left(R_{\hat{E}'_\phi}\right) + [\hat{E}_\phi(b)]\frac{\partial}{\partial r}\left(\delta(r-b)\right). \tag{2.10}$$

The first term denotes now the distributional derivative of a regular distribution associated with $\hat{E}'_\phi$ and the second term equals the jump times a dipole [6]. Absence of a dipole term on the right-hand side of (2.8) indicates that the second term vanishes, i.e. $\hat{E}_\phi$ is continuous at b. Equation (2.8) splits now into tow equations:

- the regular distribution part,

$$\hat{E}_\phi\left(-\alpha^2 + \frac{1}{r^2}\right) - \frac{1}{r}\hat{E}'_\phi - \hat{E}''_\phi = 0; \tag{2.11}$$

- the singular distribution part

$$-\delta(r-b)\,[\hat{E}'_\phi(b)] = -\frac{i\omega\mu}{\sqrt{2\pi}}\delta(r-b). \tag{2.12}$$

Equation (2.11) is the Bessel equation for which a solution argument must be scaled by factor α [7]. We split our $1D$ domain into two intervals (a,b) and $(b,+\infty)$. The solution over each interval is a linear combination of the Hankel functions of the first and the second type,

$$\hat{E}_\phi^{(a,b)} = C_1 H_1^{(1)}(\alpha r) + C_2 H_1^{(2)}(\alpha r), \tag{2.13}$$

$$\hat{E}_\phi^{(b,+\infty)} = C_3 H_1^{(1)}(\alpha r) + C_4 H_1^{(2)}(\alpha r). \tag{2.14}$$

We need to determine now the four coefficients C_1, C_2, C_3 and C_4.

The first condition to be used is the jump condition (2.12).

Moreover, we assume that the metallic mandrell is a perfect conductor. With the electric field vanishing in a perfect conductor, and the tangential component of E being continuous across material interfaces, the tangential component of E on a boundary adjacent to a perfect conductor must vanish [8] $n \times \hat{E}_\phi = 0$. In our case this simply translates into the condition,

$$\hat{E}_\phi^{(a,b)}(a) = 0. \tag{2.15}$$

The third condition enforces the continuity of $\hat{E}_\phi$ at b,

$$\hat{E}_\phi^{(a,b)}(b) = \hat{E}_\phi^{(b,+\infty)}(b). \tag{2.16}$$

The fourth condition is associated with the asymptotic behavior of Hankel functions [5]. It follows that the Hankel function of the first order $H_1^{(1)}(\alpha(\hat{z})\, r)$ tends to 0 when the imaginary part of $\alpha(\hat{z})$ goes to infinity, whereas the Hankel functions of the second order $H_1^{(2)}(\alpha(\hat{z})\, r)$ blows up to infinity, when the imaginary part of $\alpha(\hat{z})$ goes to infinity. This implies that $C_4 = 0$.

3 Closed form solution

We solve now the system of three equations (2.12), (2.15) and (2.16) with three unknowns C_1, C_2, C_3. The solution is,

$$C_1 = -C_2 \frac{H_1^{(2)}(\alpha a)}{H_1^{(1)}(\alpha a)}, \tag{3.17}$$

$$C_2 = -\frac{\sqrt{\pi} b\omega\mu}{4\sqrt{2}} H_1^{(1)}(\alpha b), \tag{3.18}$$

$$C_3 = \frac{\sqrt{\pi} b\omega\mu}{4\sqrt{2}} \left(H_1^{(2)}(\alpha b) - \frac{H_1^{(2)}(\alpha a)}{H_1^{(1)}(\alpha a)} H_1^{(1)}(\alpha b) \right). \tag{3.19}$$

Therefore, the angular component of the electromagnetic field in the Fourier domain is,

$$\hat{E}_\phi^{(a,b)}(r) = -\frac{\sqrt{\pi} b\omega\mu}{4\sqrt{2}} \left(H_1^{(1)}(\alpha b)\, H_1^{(2)}(\alpha r) - \frac{H_1^{(1)}(\alpha r)\, H_1^{(2)}(\alpha a)\, H_1^{(1)}(\alpha b)}{H_1^{(1)}(\alpha a)} \right), \tag{3.20}$$

and

$$\hat{E}_\phi^{(b,+\infty)}(r) = \frac{\sqrt{\pi} b\omega\mu}{4\sqrt{2}} \left(H_1^{(2)}(\alpha b)\, H_1^{(1)}(\alpha r) - \frac{H_1^{(2)}(\alpha a)}{H_1^{(1)}(\alpha a)} H_1^{(1)}(\alpha b)\, H_1^{(1)}(\alpha r) \right). \tag{3.21}$$

In deriving (3.18), (3.19) and (3.20) we have used the Wronskian formula for Hankel functions [10],

$$H_1^{(2)}(\alpha r)\, H_2^{(1)}(\alpha r) - H_1^{(1)}(\alpha r)\, H_2^{(2)}(\alpha r) = -\frac{4i}{\pi r}. \tag{3.22}$$

We use the scaled Hankel functions, in order to eliminate indeterminate symbols,

$$H_1^{(1)}(z) = \bar{H}_1^{(1)}(z) \exp(-zi), \tag{3.23}$$

$$H_1^{(2)}(z) = \bar{H}_1^{(2)}(z) \exp(zi). \tag{3.24}$$

The final formulae for the solution in the Fourier domain are,

$$\hat{E}_\phi^{(a,b)}(r) = -\frac{\pi b\omega\mu}{4\sqrt{2}} \left(\bar{H}_1^{(1)}(\alpha b)\, \bar{H}_1^{(2)}(\alpha r) \exp(-\alpha i(r-b)) \right.$$

$\hat{z}$	$\sqrt{r_1}$	$\frac{\theta_1}{2}$	$\sqrt{r_2}$	$\frac{\theta_2}{2}$
$-\infty$	$+\infty$	$\frac{\pi}{2}$	$+\infty$	$-\frac{\pi}{2}$
0	$\sqrt{r_0}$	$\frac{\theta_0}{2}$	$\sqrt{r_0}$	$-\frac{\theta_0}{2}$
$+\infty$	$+\infty$	$\frac{\pi}{2}$	$+\infty$	$-\frac{\pi}{2}$

Table 1: Two branches of $\alpha(\hat{z}) = +/-\sqrt{r}\exp i\frac{\theta}{2}$.

$$-\frac{\bar{H}_1^{(1)}(\alpha r)\,\bar{H}_1^{(2)}(\alpha a)\,\bar{H}_1^{(1)}(\alpha b)}{\bar{H}_1^{(1)}(\alpha a)}\exp\left(-\alpha i(2a-b-r)\right)\Bigg), \tag{3.25}$$

where $a < r < b$, and,

$$\hat{E}_\phi^{(b,+\infty)}(r) = \frac{\sqrt{\pi}b\omega\mu}{4\sqrt{2}}\Big(\bar{H}_1^{(2)}(\alpha b)\,\bar{H}_1^{(1)}(\alpha r)\exp\left(-\alpha i(r-b)\right)$$

$$-\frac{\bar{H}_1^{(2)}(\alpha a)}{\bar{H}_1^{(1)}(\alpha a)}\bar{H}_1^{(1)}(\alpha b)\,\bar{H}_1^{(1)}(\alpha r)\exp\left(-\alpha i(b+r-2a)\right)\Bigg), \tag{3.26}$$

where $a < b < r$.

4 Numerical implementation

We have used the goal-oriented *hp* adaptive code to compute the solution at a sequence of points $(r = b, z = z_n)$, where $z_n \in (0.5, 3.5)$ meters. The point source has been replaced with a small finite size antenna. As the evaluation of the analytical solution becomes unstable for r close to b, we have replaced $r = b$ with $r = a + (b-a) * 0.99$. Fig. 2 presents the real and imaginary parts of the solution as a function of $\hat{z}$ for the selected value of r.

There are two essential components of the numerical evaluation of the analytical solution:

- numerical evaluation of the scaled Hankel functions,
- numerical evaluation of the inverse Fourier transform.

Both steps have been implemented in MATLAB.

4.1 Evaluation of Bessel functions

The argument for all Bessel functions of the third kind (Hankel functions) assumes complex values αr, where $\alpha = (k^2 - \hat{z}^2)^{\frac{1}{2}}$ where $k^2 = \mu\omega^2\epsilon - \mu\sigma\omega i$. There are two branches of the complex root $+/-\sqrt{|k^2-\hat{z}^2|}\exp i\frac{\theta}{2}$, where θ depends upon $\hat{z}$, as illustrated in Fig. 3 and Table 1. The selection of the branch affects the asymptotic behavior of the solution in the Fourier domain as $|\hat{z}| \to \infty$, and

it corresponds to the elimination of $H_1^{(2)}(\alpha(\hat{z}), r)$, see the discussion in the previous section. The Hankel functions are computed by using MATLAB routine *besselh*(μ,K,Z,1) [9] using algorithms described in [10].

4.2 Evaluation of Fourier transform using FFT

The inverse FFT is used to approximate the integral,

$$E_\phi(r,z) = \frac{1}{2\pi}\int_{-\infty}^{+\infty} \chi(\hat{z})\,\hat{E}_\phi(r,\hat{z})\exp(iz\hat{z})\,d\hat{z}, \tag{4.27}$$

at a sequence of points, where χ denotes a truncating function defined below. The integral is computed numerically by selecting a window $\left[-\hat{b},\hat{b}\right]$ in the Fourier domain, and using a discrete approximation,

$$E_\phi(r,z) \approx \frac{1}{2\pi}\int_{-\hat{b}}^{+\hat{b}} \chi(\hat{z})\,\hat{E}_\phi(r,\hat{z})\exp(iz\hat{z})\,d\hat{z} \approx \frac{1}{2\pi}\sum_{j=1}^{2N} \chi(\hat{z}_j)\,\hat{E}_\phi(r,\hat{z}_j)\exp(iz\hat{z}_j)\,d\hat{z}, \tag{4.28}$$

with a sequence of points,

$$\hat{z}_j = \frac{\Delta\hat{z}}{2} - N\Delta\hat{z} + (j-1)\,\Delta\hat{z}, \tag{4.29}$$

for $j = 1, ..., 2N$. The inverse FFT,

$$E_\phi(r,z_k) = \frac{1}{2\pi}\sum_{j=1}^{2N} \chi(\hat{z}_j)\,\hat{E}_\phi(r,\hat{z}_j)\exp(iz_k\hat{z}_j)\,d\hat{z}, \tag{4.30}$$

is computed at a sequence of points,

$$z_k = \frac{\Delta z}{2} - N\Delta z + (k-1)\,\Delta z. \tag{4.31}$$

The size of the real domain window $[-b,b]$ can be computed from relations,

$$\Delta\hat{z}\Delta z = \frac{\pi}{N} \text{ and } b\hat{b} = \pi N. \tag{4.32}$$

There are three general observations concerning the accuracy of the inverse FFT

- A twofold increase of the window size in the Fourier domain $\left[-2\hat{b},2\hat{b}\right]$, under a fixed number of points N, causes the real domain window to decrease twofold $\left[-\frac{1}{2}b,\frac{1}{2}b\right]$.
- A twofold increase of the number of points $2N$, under a fixed size of the Fourier domain window, causes the real domain window to increase twofold $[-2b,2b]$.
- A simultaneous twofold increase of the window size in the Fourier domain $\left[-2\hat{b},2\hat{b}\right]$, with the number of points $2N$ doubled, increases the accuracy with the real domain window size remaining fixed.

The convergence of the inverse FFT in the third regime is illustrated in Fig. 4.

Two choices of the truncating function χ have been investigated. Results obtained with a simple characteristic function $\chi = 1_{[-\hat{b},\hat{b}]}$ converge very slowly and do not match the FE computations, see Fig. 5.

The reason is that the integrated function along with its derivatives must be smooth over the complex circle.

Following the ideas of Bruno at al. [1], we truncate the Fourier integral with a C_0^∞ function (see Fig. 6) given by,

$$\chi\left(\hat{z}\right) = \begin{cases} \exp\left(\frac{1}{1-\left(\frac{\hat{z}-(-b+\hat{\epsilon})}{\hat{\epsilon}}\right)}\right) & \text{for } \hat{z} \in \left[-\hat{b}, -\hat{b}+\epsilon\right] \\ 1 & \text{for } \hat{z} \in \left(-\hat{b}+\epsilon, \hat{b}-\epsilon\right) \\ \exp\left(\frac{1}{1-\left(\frac{\hat{z}-(b-\hat{\epsilon})}{\hat{\epsilon}}\right)}\right) & \text{for } \hat{z} \in \left[\hat{b}-\epsilon, \hat{b}\right] \end{cases} , \tag{4.33}$$

where $\epsilon = \frac{\hat{b}}{4}$. Application of the truncating smooth function (4.33) results in a fast (exponential ?) convergence of the inverse FFT, as presented in Fig. 7.

The results obtained with the smooth truncating function match perfectly the numerical results obtained with the goal-oriented *hp* adaptive strategy, see Fig. 8.

5 Conclusions

The paper presents a "struggle" with a numerical evaluation of the inverse Fourier transform. We have shown that truncating the solution in the Fourier domain with a C_0^∞ function, guarantees a fast and efficient evaluation of Fourier integral using FFT. The resulting integrand is C^∞ over the complex circle, which enables a fast (exponential ?) convergence.

The presented results provide an additional proof for the unprecedented accuracy obtainable with the goal-oriented *hp* adaptivity.

A copy of the MATLAB code can be requested from the first author.

References

[1] O. Bruno, C. Geuzaine, F. Reitich "A new high-order high-frequency integral equation method for the solution of scattering problems", *Proceedings of the 20th Annual Review of Progress in Applied Computational Electromagnetics*, Syracuse, New York, (2004)

[2] D. Pardo, L. Demkowicz, C. Torres-Verdin, L. Tabarovsky, "A Goal Oriented *hp*-Adaptive Finite Element Strategy with Electromagnetic Applications. Part I: Electrostatics.", Submitted to: *International Journal for Numerical Methods in Engineering*, (2004)

[3] J. R. Lovell, *Finite Element Methods in Resistivity Logging*, Delft University of Technology, (1993), p.38-45

[4] M.D. Greenberg, *Foundations of Applied Mathematics*, Prentice-Hall International, (1978)

[5] N. N. Lebedev, *Special Functions and Their Applications* , Dover Publications, New York, (1972)

[6] A.H. Zemanian, *Distribution Theory and Transform Analysis: An Introduction to Generalized Functions, With Application*, Dover Publications, New York, (1965)

[7] J. S. Walker, *Fourier Analysis*, Oxford University Press, New York, (1988)

[8] L. Demkowicz, "Finite Element Methods for Maxwell Equations", *Encyclopedia of Computational Mechanics*, John Wiley & Sons, (2004)

[9] MATLAB User Guide

[10] M. Abramowitz, I. A. Stegun, *Handbook of Mathematical Functions*, National Bureau of Standards, Applied Math. Series #55, Dover Publications, (1965)

[11] J. T. Oden, L. Demkowicz, *Applied Functional Analysis*, CRC Press, 1996

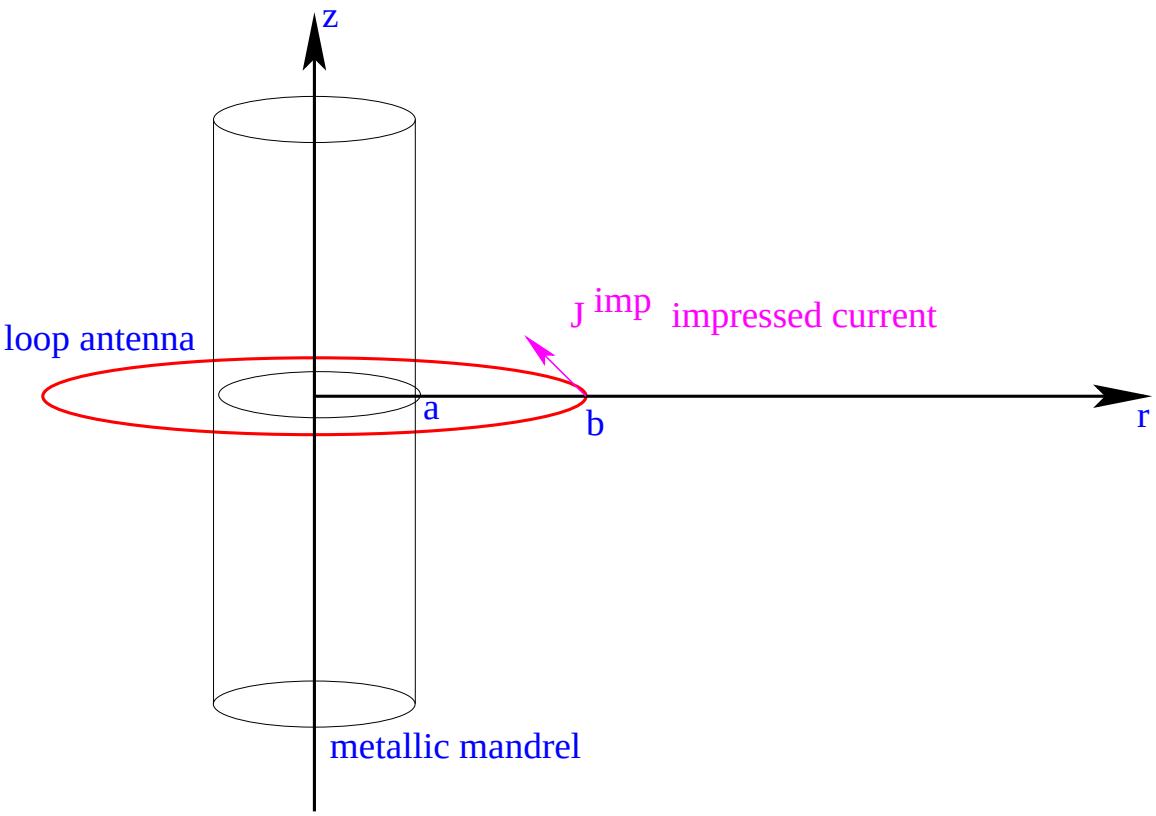

Figure 1: Configuration of the metallic mandrel and loop antenna

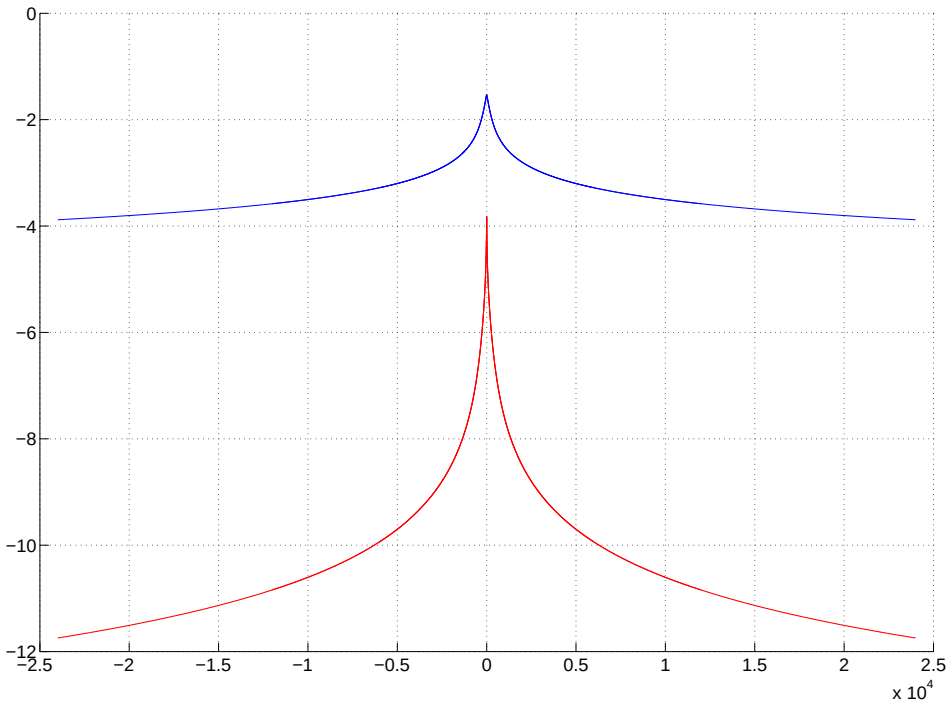

Figure 2: Analytic solutions for $r = (a + (b - a) * 0.99)$. Red color denotes a real part, blue color denotes an imaginary part.

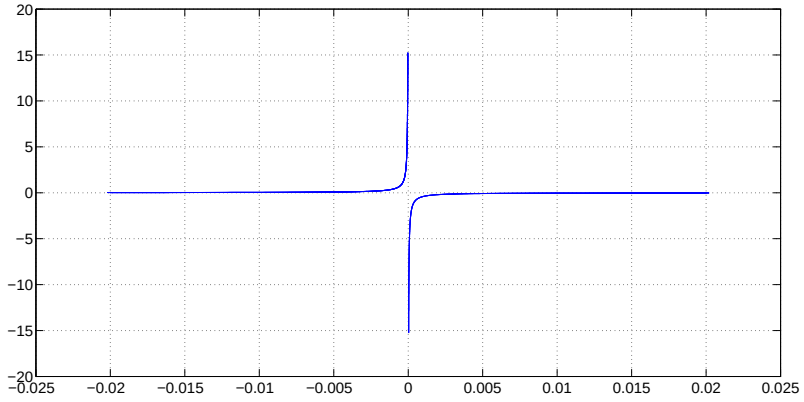

Figure 3: Two branches of $\alpha\hat{z} = +/- \sqrt{r} \exp i\frac{\theta}{2}$. Vertical axis denotes real part of $\alpha\hat{z}$, horizontal axis denotes imaginary part of $\alpha\hat{z}$.

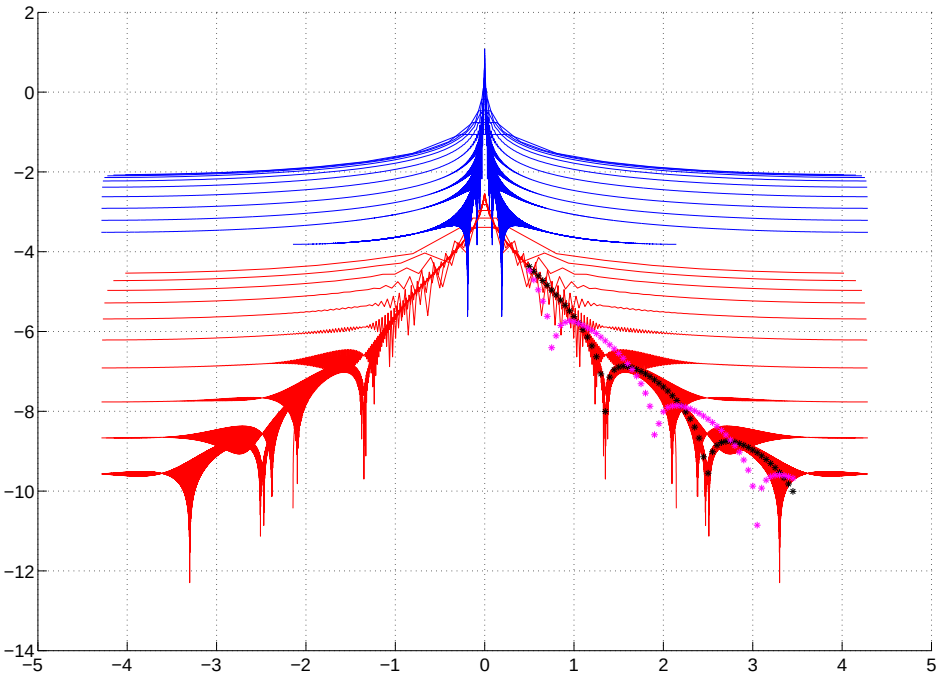

Figure 4: Convergence of the inverse Fourier transform using FFT without truncating function $\chi = 1_{[-\hat{b},\hat{b}]}$, for $N = 2^{5,6,...,11,12}$ and $\hat{b} = 3000{*}2^{-7,-6,-5,...,-1,0}$. Vertical axis = log_{10}(Electromagnetic field); Horizontal axis = distance [m]. Red color denotes a real part, blue color denotes imaginary part of the solution. Black stars denote real part of the goal-oriented *hp* adaptive result, pink stars denote its imaginary part.

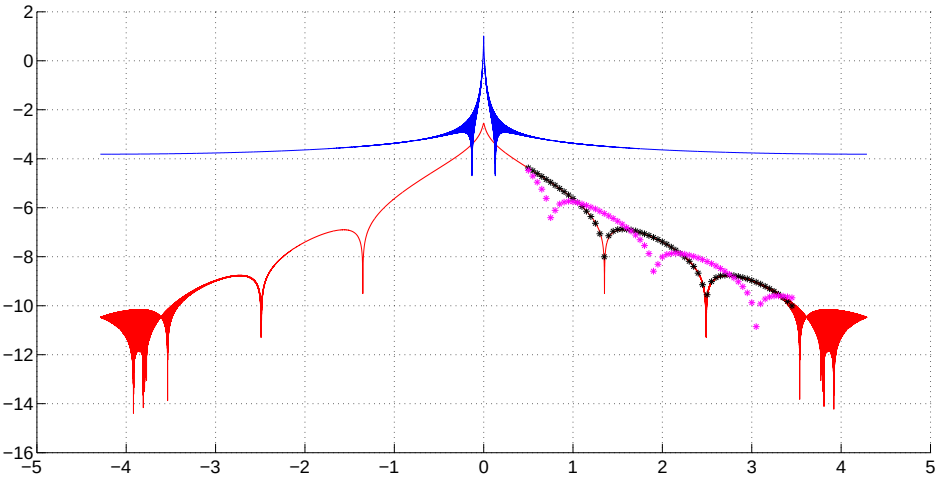

Figure 5: Comparison of the inverse Fourier transform using FFT without truncating function $\chi = 1_{[-\hat{b},\hat{b}]}$ with the results of goal-oriented *hp* adaptive computations. Vertical axis = log_{10}(Electromagnetic field); Horizontal axis = distance [m]. Red color denotes a real part, blue color denotes imaginary part of the solution. Black stars denote real part of the goal-oriented *hp* adaptive result, pink stars denote its imaginary part.

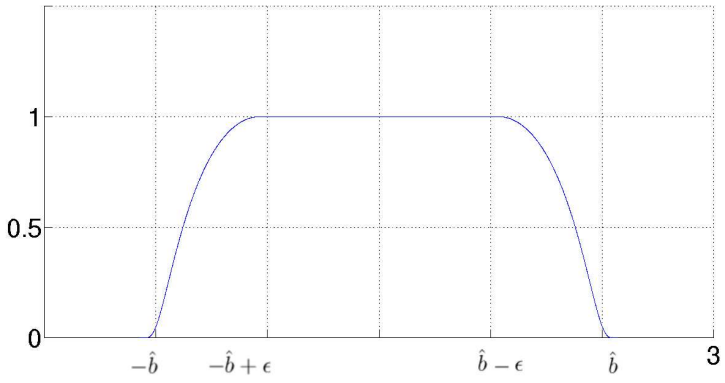

Figure 6: Truncating function χ

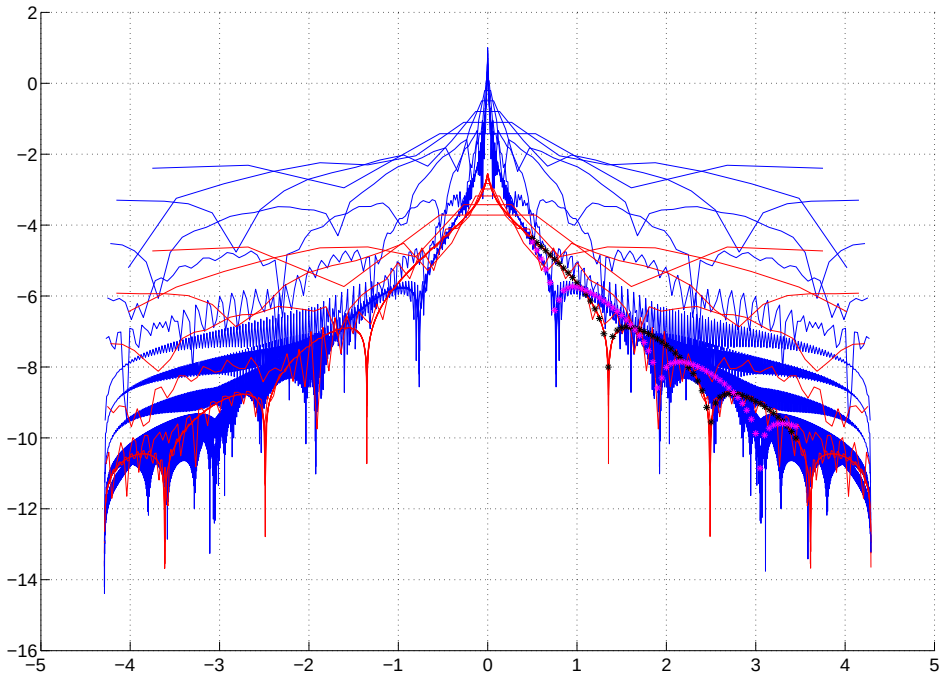

Figure 7: Convergence of the inverse Fourier transform using FFT with the smooth truncating function χ given by (4.33), for $N = 2^{5,6,\ldots,11,12}$ and $\hat{b} = 3000 * 2^{-7,-6,-5,\ldots,-1,0}$. Vertical axis = log_{10}(Electromagnetic field); Horizontal axis = distance [m]. Red color denotes a real part, blue color denotes imaginary part of the solution. Black stars denote real part of the goal-oriented *hp* adaptive result, pink stars denote its imaginary part.

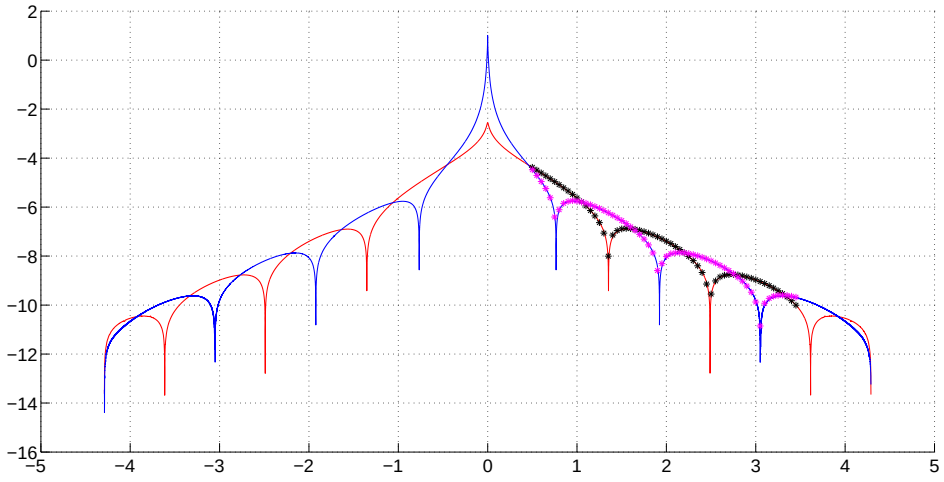

Figure 8: Comparison of the inverse Fourier transform using FFT with truncating function χ given by (4.33) with the results of goal-oriented hp adaptive computations. Vertical axis = log_{10}(Electromagnetic field); Horizontal axis = distance [m]. Red color denotes a real part, blue color denotes imaginary part of the solution. Black stars denote real part of the goal-oriented hp adaptive result, pink stars denote its imaginary part.